

Visual investigation of the domain structure of ferrimagnetic RbNiF_3

A. I. Belyaeva, S. V. Petrov,¹⁾ Yu. N. Stel'makhov, and V. P. Yur'ev

Physicotechnical Institute of Low Temperatures, Ukrainian Academy of Sciences

(Submitted 12 May 1980)

Zh. Eksp. Teor. Fiz. 79, 2252–2262 (December 1980)

The domain structure of a hexagonal ferromagnet was investigated with RbNiF_3 as the example. The behavior of the structure was studied in the temperature interval 140–4.2 K and in external magnetic fields of different geometry. The distinguishing features of the formation of the domain structure are investigated in a hexagonal ferrimagnet with anisotropy of the easy plane type, when the anisotropy constant K_3 is small and the important role in the formation of the domain structure is played by internal elastic stresses of nonmagnetic origin. Thermodynamic models that explain the main features of the experimentally observed domain structure are proposed.

PACS numbers: 75.60.Ch, 75.50.Gg

It is known that the appearance of a spontaneous magnetic moment at $T < T_{\text{cr}}$ is accompanied by breakup of a ferrimagnetic sample into a number of uniformly magnetized regions (domains) separated by domain walls. The domain structure (DS) of magnetically uniaxial crystals has been investigated in sufficient detail both theoretically and experimentally. In the case of multiaxial crystals, owing to the great variety of DS that are produced in them, the problem becomes greatly complicated. Whereas the DS of multiaxial cubic ferrimagnets is being quite diligently investigated in the last few years (see, e.g., Ref. 1), the laws governing its formation in the case of hexagonal crystals with anisotropy of the easy plane type has not been investigated to this day. The greatest opportunities for a correct interpretation of the DS and for the understanding of the mechanism of its restructuring in a magnetic field are offered by transparent crystals with a DS that permeates through the entire sample and is revealed by magneto-optical effects.

The ionic ferrimagnet RbNiF_3 is transparent to visible light. Among its unusual magnetic properties are the large magnitude, of the same order of the linear magneto-optical Faraday effect and of the quadratic Cotton-Mouton effect.² These properties enabled us in the present study to observe visually the formation of the DS that is produced when RbNiF_3 undergoes a phase transition into the ferrimagnetic state, and to study its behavior in the temperature interval 140–4.2 K and in external magnetic fields with various geometries. Indirect arguments favoring the presence of a DS in ferrimagnetic RbNiF_3 were advanced earlier.^{3,4} The study of the DS is of very great importance for the understanding of all the magnetic properties of ferrimagnetic RbNiF_3 . It is also obvious that to study these properties one must know how to obtain a single-domain state wherein a single spin-ordering axis is realized in the entire volume.

In the interval from room temperature to 30 K, RbNiF_3 has a hexagonal structure and its symmetry is described by the space group D_{6h}^4 .^{5,6} Six nickel ions

occupy in the unit cell two non-equivalent positions NiA(2) and NiB(4). Below $T_{\text{cr}} = 139$ K, RbNiF_3 is a six-sublattice collinear uncompensated antiferromagnet (ferrimagnet) with anisotropy of the easy plane type.⁶ The anisotropy in the basal plane is less than 10 Oe.⁷ The spins are arranged perpendicular to the hexagonal axis C_6 in ferromagnetic planes made up of like ions in such a way that the spins in the neighboring planes belong to the neighboring sublattices A and B:

$$\text{NiA}(+), \text{NiB}(-), \text{NiB}(-), \text{NiA}(+), \text{NiB}(-), \text{NiB}(-).$$

The signs (+) and (–) refer to opposite directions of the spins in space. The presence of a resultant ferromagnetic moment leads us to expect the appearance of a DS when the crystal goes over into a magnetically ordered state.

Single crystals of RbNiF_3 ($T_{\text{melt}} = 984 \pm 5^\circ\text{C}$) used in the present investigation were grown at the Institute of Physics Problems of the USSR Academy of Sciences by the Bridgmann method in an atmosphere of helium vapor from a dewar, in thin-wall (0.05 mm) platinum crucibles. The crystals were transparent, green, without any cracks, inhomogeneities or bubbles, and contained no blocks. X-ray investigations have shown that their structure is hexagonal with room-temperature lattice parameters $a = 5.843 \text{ \AA}$ and $c = 14.310 \text{ \AA}$ close to those known from the literature.⁸ The samples were produced from oriented RbNiF_3 single crystals, and their surfaces were optically ground and polished. A special check has shown that this procedure obviates the need for annealing, since the layer deformed by the finishing is very thin compared with the sample thickness and introduces no significant errors in the experimental results. We investigated single-crystal samples whose developed plane coincided with the basal plane of the crystal or was perpendicular to it. The accuracy of the orientations of the planes and of the sixfold and twofold in them was not worse than 1° . Similar experimental results were obtained for control samples grown by P. P. Syrkin at the A. F. Ioffe Physicotechnical Institute.

The DS were investigated by magneto-optical methods. Visual observation of the DS was by a setup analogous to that described in Ref. 9. The light source was a DKSSh-120 xenon lamp. There were no phase plates in the optical system. For the investigations in the temperature interval 140–4.2 K the sample was placed in a special flow-through cryostat of the type described in Ref. 10. Magnetic fields of various relative orientations were produced by a superconducting solenoid.

1. EXPERIMENTAL RESULTS

Figure 1 shows photographs of the DS of ferrimagnetic RbNiF₃, obtained for one sample in the form of a rectangular parallelepiped with edges parallel to the crystallographic axes, in three experimental geometries:

a) Light (k) perpendicular to the crystal hexagonal axis C_6 (nonaxial geometry, crystal thickness 2 mm along k): $k \parallel C_2'$; $E \parallel C_2$; E is the electric vector of the light wave.

b) Light (k) perpendicular to the C_6 axis (nonaxial geometry, crystal thickness 2 mm): $k \parallel C_2$; $E \parallel C_2'$.

c) Light (k) parallel to hexagonal axis C_6 (axial geometry, crystal thickness 3.5 mm): $k \parallel C_6$; $E \parallel C_2$ (C_2').

In the first two (nonaxial) cases the magneto-optical contrast is determined by a complicated combination of the Faraday and birefringence effects in the inhomogeneity magnetized medium.¹¹ In the axial geometry there is no Faraday effect, and the spontaneous magnetic birefringence appears against a zero background, since there is no natural birefringence in the C_6 direction.

In all three cases of Fig. 1, the DS is very complicated and does not pass through the entire sample. In the case of nonaxial geometry of the crystals of Figs. 1a and 1b it is obvious, however, that there are domain walls of two types: parallel to the C_6 axis and parallel to the basal plane. The character of the DS is independent of which of the symmetry axes, (C_2 or C_2'), lies in the plane of the crystal. For axial geometry, Fig. 1c, one can clearly see macrodomains with various orientations, containing strip microdomains whose directions in the different macrodomains can be at angles 60° or 120° to each other. The wedge shape of the macrodomains, which is typical of crystal twins, is evidence of a substantial influence of the magneto-

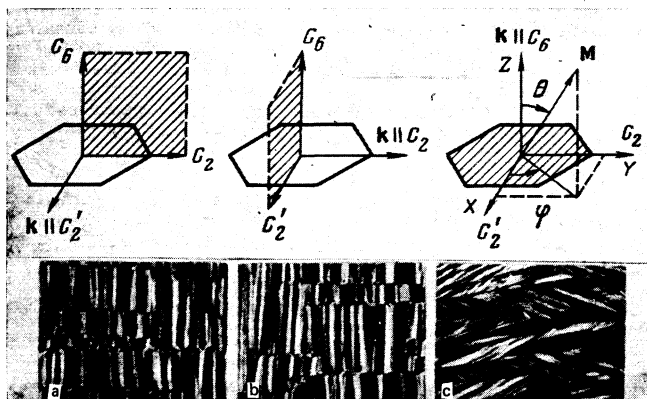


FIG. 1. DS of RbNiF₃ at $T = 40$ in three experimental geometries.

striction strains and elastic stresses on the relative arrangement of the ferrimagnetic domains. The DS of Fig. 1 is very mobile in a magnetic field parallel to the axes C_2 and C_2' , and vanishes completely in fields $H_s = (430 \pm 10)$ Oe. Investigations of the character of the DS and of its behavior in an external magnetic field, however, did not make it possible to assess the anisotropy in the basal plane; Figs. 1a and 1b (C_2 and C_2' axes) turn out to be equivalent. It is easy to show that the saturation field H_s in this case, in view of the low anisotropy energy in the basal plane, is completely determined by the demagnetizing field of the sample at $M_0 \parallel H_s$. Approximating the shape of the sample by an ellipsoid with principal axes 2, 2, and 3.5 mm, we obtain at a saturation magnetization $M_0 \approx 81.5$ G (Ref. 6):

$$H_s \approx 0.4 \cdot 4\pi M_0 = 410 \text{ Oe,}$$

which is in sufficient agreement with the experimental value.

It is seen from Fig. 1 that the DS of a multiaxial thick RbNiF₃ crystal is quite complicated. To understand the main regularities of its formation we have investigated a thin plate (thickness $h = 80 \mu\text{m}$) in a geometry analogous to that of Fig. 1a. Figure 2 shows the changes of the DS in such a plate in the temperature range 140–4.2 K. It is obvious that the appearance of optical contrast (DS) at $T < 140$ K is determined by the phase transition due to the establishment of magnetic order in the crystal ($T_{cr} = 139$ K, Ref. 6). The optical contrast increases when the temperature is lowered in the interval $140 > T > 70$ K, and then remains constant at temperatures $70 > T \geq 4.2$ K. The temperature dependence of the optical contrast can be naturally attributed to the temperature dependence of the spontaneous magnetic moment and to the spontaneous lattice deformation associated with this moment (magnetostriction), which in all probability is responsible for the magnetic birefringence. The DS changes little with

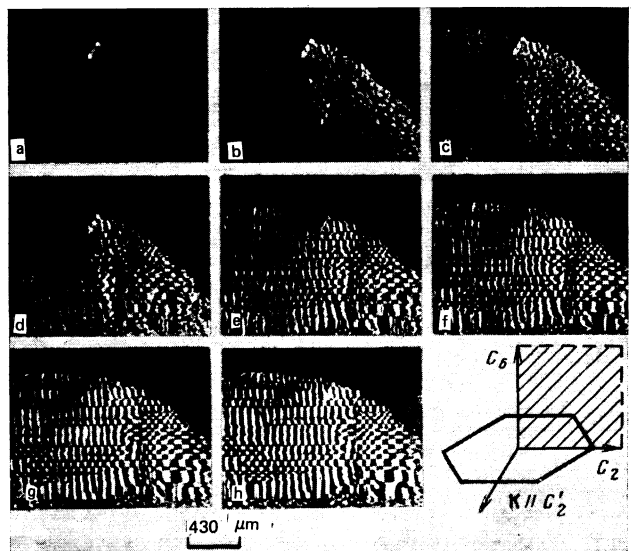


FIG. 2. DS in nonaxial plate of RbNiF₃ at various temperatures (K): a) 140, b) 138, c) 135, d) 130, e) 110, f) 90, g) 70, h) 40–4.2. Plate Thickness $h = 80 \mu\text{m}$.

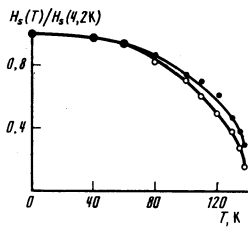


FIG. 3. Temperature dependence of the field H_s (in relative units) at which the DS vanishes: ● $H \parallel C'_2 \parallel k$; ○ $H \parallel C_2 \parallel k$.

changing temperature. After heating and second cooling, its main features remain the same. No temperature hysteresis was observed. Investigations of the plate from both sides using an objective with a low depth of focus, which made it possible to trace the DS over the entire thickness of the plate, has shown that the DS of Fig. 2 permeates through the entire plate.

We note the following features of the DS in a nonaxial plate of magnetically disordered RbNiF_3 (Fig. 2h). The sample is broken up into layers of various widths parallel to the basal plane. Inside the layers the DS is quite regular and can be interpreted with good accuracy as a strip structure with domain walls parallel to the C_6 axis. Any irregularities can be due to imperfections in the crystal. The period of the strip DS in the layers is somewhat different in different regions of the crystal and amounts on the average to $P_{av} = 2d \approx 40 \mu\text{m}$ ($d \approx 20 \mu\text{m}$ is the domain size). A tendency to form a DS of the "checkerboard" type is evident on the boundary between the layers.

A substantial anisotropy was observed in the behavior of the DS in a magnetic field parallel to different two-fold axes, and obviously determined by the shape of the plate. The sample goes over into a uniformly magnetized state (the DS vanishes) in fields $H \approx 115 \text{ Oe}$ ($H \parallel C_2$, in the plane of the plate) and $H \approx 700 \text{ Oe}$ ($H \parallel C'_2$, perpendicular to it). Figure 3 illustrates the temperature dependence of the fields at which the DS vanishes.

The DS turned out to be very stable in a magnetic field parallel to the C_6 axis. In this case, however, owing to the inexact orientation of the field, the latter can have a component in the basal plane, which also sets up moments along one direction that coincides with

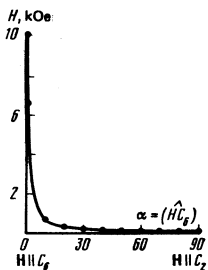


FIG. 4. Magnetic field in the plate plane, needed to obliterate the DS, vs. the angle between the field and the hexagonal axis of the crystal. Experimental geometry of the type of Figs. 1a and 1b. $T = 40 \text{ K}$. Points—results of experiment; solid curve—calculation for saturation field $H_s = 115 \text{ Oe}$ in the basal plane.

the projection of the field on this plane. At an inclination $\sim 40'$ and at a saturation field in the basal plane $\sim 115 \text{ Oe}$, this transition to the one-domain state takes place at $H \approx 10 \text{ kOe}$, in agreement with experiment. Figure 4 shows a comparison of the calculation with experiment for the saturation field as a function of the angle of its deviation from the C_6 axis. The agreement demonstrates that in fields up to 10 kOe there is no rotation of the magnetic moment on the basal plane. The vanishing of the DS is connected with the projection of the magnetic field on this plane. Estimates show that the saturation field of the RbNiF_3 sample in the direction of the C_6 axis, a field determined mainly by the first anisotropy constant $K_1 \sim 6 \times 10^5 \text{ erg/cm}^3$,⁷ amounts to

$$H_s \approx 2K_1/M_0 = 15 \text{ kOe}.$$

2. DISCUSSION OF EXPERIMENTAL RESULTS AND MODEL OF DOMAIN STRUCTURE

The DS of the crystal can be theoretically predicted by minimizing its total energy. In the case of RbNiF_3 this is too complicated a problem and has no real solution. We shall therefore attempt to construct a DS model and ascertain the nature of its formation, taking into account the distinguishing features experimentally observed in the DS of ferrimagnetic RbNiF_3 . The minimization of the energy of such a model can yield the principal parameters of the most realistic DS. To this end we determine first the equilibrium orientations of the magnetic moment in the domains of ferrimagnetic RbNiF_3 and the orientations of the domain walls.

A. Orientation of magnetic moment in domains

The equilibrium orientations of the magnetic moment in the domains are determined from the condition that the energy density of the magnetic anisotropy be a minimum¹²:

$$E_{\kappa\sigma_i}(\theta, \varphi) = E_{\kappa}(\theta, \varphi) + E_{\sigma_i}(\theta, \varphi), \quad (1)$$

where

$$E_{\kappa}(\theta, \varphi) = K_1 \cos^2 \theta + K_2 \cos^4 \theta + K_3 \sin^4 \theta \cos 6\varphi$$

is the energy density of the natural magnetic anisotropy; $E_{\sigma_i}(\theta, \varphi)$ is the energy density of the residual elastic stresses of nonmagnetic origin at the given point of the crystal; θ and φ are the polar and azimuthal angles of the magnetization vector in a spherical coordinate system (Fig. 1c).

For RbNiF_3 we have $K_1 > 0, K_2 > 0, |K_1| \gg |K_2| \gg |K_3|$,⁷ but the sign and magnitude of the constant K_3 , as well as the distribution of the residual internal stresses, are unknown. It is therefore advisable to examine the possible cases and choose the most realistic among them:

1. If $|K_1| \gg |K_2| \gg |K_3|$, $|E_{\sigma_i}|$, then at each point of the crystal there exist six directions of easy magnetization (or three easy-magnetization axes—EMA), which are characterized, depending on the sign of K_3 , by the angles

$$\begin{aligned} \theta = \pi/2, \quad \varphi = (2n+1)\pi/6 & \text{ at } K_3 > 0, \text{ EMA } -C_2; \\ \theta = \pi/2, \quad \varphi = n\pi/3 & \text{ at } K_3 < 0, \text{ EMA } -C'_2. \end{aligned} \quad (2)$$

In this case, six equilibrium orientations of the magnetic moment can coexist, and we can consequently expect a closed hexagonal (or triangular) DS to be energy-wise more favored.^{1,4}

2. If $|K_1| \gg |K_2| \gg |E_{\sigma_i}| \gg |K_3|$, then at each point of the crystal there exists only one EMA which, as in the first case, is characterized by an angle $\theta = \pi/2$, but the angle φ is determined by the minimum of the energy E_{σ_i} .

3. If K_3 or E_{σ_i} are comparable in magnitude, then to determine the EMA and their number we must know the magnitude and direction of the residual stresses. In the particular case when E_{σ_i} is smaller than K_3 , the easy magnetization axes can be one or two axes of the natural magnetic anisotropy (3), which are most favored from the point of view of the energy E_{σ_i} .

Visual observation of the DS in RbNiF₃ revealed no closed hexagonal or triangular structures. The macrodomains observed in the axial geometry of the experiment (Fig. 1c) can be interpreted as regions of tension or compression, in which one or two EMA appear. The presence of microstrip DS inside the macrodomains is evidence that the characteristic dimensions of the tension (compression) regions exceed the dimensions of the domains.¹² The directions of the microstrip structures in different macrodomains can make angles 60 or 120° with each other (Fig. 1c). This proves that the EMA in the macrodomains are close to the axes of the natural magnetic anisotropy. The DS observed in the two nonaxial geometries (Figs. 1a and 1b) are qualitatively the same, thus confirming once more that the residual stresses influence the formation of DS in ferromagnetic RbNiF₃.

Thus, the experimentally observed features of the DS in RbNiF₃ allow us to state that the EMA in the different regions of the crystal are one or two of the natural-magnetic-anisotropy easy axes that are most favorable from the point of view of the residual stresses. In those crystal regions where $|E_{\sigma_i}| \ll |K_3|$, the EMA may deviate from the natural magnetic anisotropy axes.

B. Domain walls

To make the model of the DS in RbNiF₃ concrete, we must determine the possible orientations of the domain walls. To this end we consider a plane wall between domains with magnetization directions φ_1 and φ_2 ($\varphi = \pi/2$). We assume that all the quantities in the transition layer are functions of only one coordinate. In RbNiF₃ the constant $K_1 \approx 6 \times 10^5$ erg/cm³, and $2\pi M_0^2 \approx 4 \times 10^4$ erg/cm³,^{6,7} so that it can be assumed that a positive second-order anisotropy (K_1) will keep the magnetization in the basal plane ($\theta = \pi/2$) even in the transition layer.

On the domain walls it is necessary to satisfy the condition for the coexistence of the phases.¹³ In addition, the domain wall tends to assume an orientation such that the stray fields and the magnetostriction stresses, which are produced when the magnetization is not uniformly distributed, have no long-range com-

ponents capable of increasing the energy of the crystal appreciably. These requirements can be expressed in the form

$$e_m(\varphi_1) = e_m(\varphi_2) = 0, \quad (3)$$

$$e_{\sigma_m}(\varphi_1) = e_{\sigma_m}(\varphi_2) = 0, \quad (4)$$

where $e_m(\varphi)$ is the local energy density of the stray fields produced by the wall, and $e_{\sigma_m}(\varphi)$ is the local density of the additional magnetostriction energy due to the inhomogeneity of the magnetization in the crystal. The results of Grishmanovskii *et al.*¹⁴ allow us to estimate this quantity for RbNiF₃: $e_{\sigma_m} \approx 7 \times 10^2$ erg/cm³.

The local energy density of the stray fields produced by the wall can be written in the form¹⁵

$$e_m(\varphi) = H_m^2/8\pi = 2\pi M_0^4 [(\cos \varphi - \cos \varphi)n_1 + (\sin \varphi - \sin \varphi)n_2]^2, \quad (5)$$

where $H_m = -4\pi(\mathbf{M} - \bar{\mathbf{M}})$ is the stray field and is the solution of the corresponding one-dimensional planar magnetostatic problem; $\bar{\mathbf{M}} = (\mathbf{M}_1 + \mathbf{M}_2)/2$; \mathbf{M}_1 and \mathbf{M}_2 are the magnetization vectors at the centers of neighboring domains; $n = n_1\mathbf{i} + n_2\mathbf{j} + n_3\mathbf{k}$ is the normal to the plane of the wall.

Taking (5) into account, we obtain from (3)

$$n_1/n_2 = \text{ctg}[(\varphi_1 + \varphi_2)/2]. \quad (6)$$

It should be noted that (6) is automatically satisfied when the electrodynamic conditions for domain coexistence are satisfied.¹³

Condition (4) is equivalent to equality of the tangential components of the spontaneous strains at the centers of neighboring domains,¹⁵ so that for two arbitrary tangential vectors $\mathbf{t}^{(1)}$ and $\mathbf{t}^{(2)}$ we have

$$[u_{ik}^{sp}(\varphi_1) - u_{ik}^{sp}(\varphi_2)]t_i^{(1)}t_k^{(2)} = 0, \quad (7)$$

where $u_{ik}^{sp}(\varphi_1)$ and $u_{ik}^{sp}(\varphi_2)$ are the tensors of the spontaneous strains in the centers of neighboring domains; $\mathbf{t}^{(1)}$ and $\mathbf{t}^{(2)}$ are vectors satisfying the conditions $\mathbf{t}^{(1)} \cdot \mathbf{n} = 0$ and $\mathbf{t}^{(2)} \cdot \mathbf{n} = 0$.

The spontaneous-strain tensor can be obtained by minimizing the elastic and magnetoelastic energies. In our case ($\theta = \pi/2$)

$$u_{ik}^{sp}(\varphi) = \begin{pmatrix} L + N \cos 2\varphi & N \sin 2\varphi & 0 \\ N \sin 2\varphi & L - N \cos 2\varphi & 0 \\ 0 & 0 & K \end{pmatrix}, \quad (8)$$

where

$$L = -\frac{1}{2} \frac{(b_{11} - b_{12})c_{33}}{(c_{11} + c_{12})c_{33} - 2c_{13}^2}, \quad N = -\frac{1}{2} \frac{b_{11} - b_{12}}{c_{11} - c_{12}}, \\ K = \frac{(b_{11} - b_{12})c_{13}}{(c_{11} + c_{12})c_{33} - 2c_{13}^2};$$

c_{ik} and b_{ik} are respectively the components of the tensor of the elastic constants and of the tensor of the magnetoelastic constants of the hexagonal crystal.¹⁴

The condition (7) is always satisfied if $\varphi_2 - \varphi_1 = \pm\pi$. Consequently only one condition is imposed on the orientation of 180-degree domain walls, namely $n_1/n_2 = \tan \varphi_1$, meaning that the plane of the wall is parallel to the magnetization directions in the neighboring domains.

On the other hand if $\varphi_2 - \varphi_1 \neq \pm\pi$, the conditions (6) and (7) are simultaneously satisfied in the case

$$n_1/n_2 = \text{ctg}[(\varphi_1 + \varphi_2)/2], \quad n_3 = 0.$$

This means that the plane of non-180-degree walls should be perpendicular to the basal plane and so oriented in it that

$$n_1/n_2 = \text{ctg}[(\varphi_1 + \varphi_2)/2].$$

The noted features of the domain-wall orientations were observed experimentally for RbNiF_3 . The walls between the strip domains in a layer are perpendicular to the basal plane and can be classified as Néel walls (Fig. 2). Walls not perpendicular to the basal plane ($n_3 \neq 0$) are always 180-degree walls. These are, for example, 180-degree Bloch walls between layers parallel to the basal plane (see Figs. 1a, 1b, and 2).

C. DS model in nonaxial RbNiF_3 plate

Taking into account the DS features observed in experiment (Fig. 2h) and the conclusions of Secs. 2A and 2B above, we shall construct the model of a DS in a nonaxial RbNiF_3 plate and calculate its parameters. The fact that the DS permeates through the RbNiF_3 plate means that the plate thickness h is less than the characteristic dimensions of the regions of the residual elastic tensions or compressions. The external form of the DS is different on different sections of the plate, owing to the differences between the magnitudes and directions of the internal stresses.

We consider the two most characteristic cases. Assume that in a given region of the plate the magnitudes and directions of the residual stresses are such that the easy axes are two axes of the natural magnetic anisotropy of type C_2 (see Fig. 5). Consequently, in the interior of the sample there can coexist four domain types. Since the anisotropy in the basal plane is low, one can expect the normal component of the magnetization to vanish on the surface of the sample.

Within the framework of this approximation, we propose the DS model shown in Fig. 5 and consisting of layers alternating along the C_6 axis and separated by 180-degree Bloch walls parallel to the basal plane (for the sake of clarity, the layers in the figure are separated in the C_6 direction). Each layer has a combined magnetic moment, and this is the cause of the alterna-

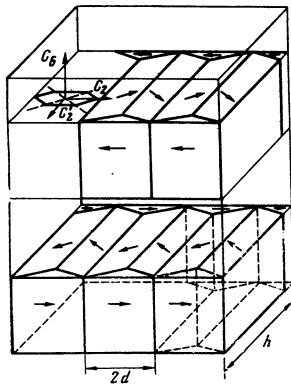


FIG. 5. Model of DS of the "checkerboard" type in a nonaxial plane. Two EMA make angles 60° and 120° with the plane of the plate.

tion of layers with oppositely oriented moments. Inside each layer the domains are separated by 120-degree Néel walls. When such a structure is observed by magneto-optical methods, it has the appearance of a checkerboard, as was in fact observed in experiment.

We estimate now the size d of the domains in the layers. The domain-wall energy (we neglect the contributions of the walls that close the domains) per unit surface of the plate is

$$E_{\sigma_{120}} \approx \sigma_{120} h/d,$$

where σ_{120} is the surface energy of a 120-degree Néel wall. Since the magnetostatic energy predominates over all other contributions to the surface energy of the wall, we have

$$\sigma_{120} \approx 2A^{3/2} \int_{\varphi_1}^{\varphi_2} e_m(\varphi) d\varphi = (2\sqrt{3} - 2\pi/3) (A \cdot 2\pi M_0^2)^{3/2},$$

where $A \approx 2J_{AB}/c\sqrt{3}$ is the effective exchange constant; $J_{AB} = 92.3$ K is the exchange integral between two nearest ions in the A and B sublattices¹⁶; c is the parameter of the hexagonal cell.

The energy of emergence of the domains to the surface of the sample is in this case the magnetostriction energy. It is very difficult to calculate accurately, but an upper bound estimate is possible.¹⁷ To this end we assume that the closing domains are subject to uniform elastic deformation by the main domains. Then the volume density of the magnetostriction energy of the closing domains is

$$\approx 3(b_{11} - b_{12})^2/4(c_{11} - c_{12}),$$

amounting per unit plate surface

$$E_{\sigma_m} = \frac{3(b_{11} - b_{12})^2}{4\sqrt{3}(c_{11} - c_{12})}.$$

The equilibrium domain size d , determined by the minimum of the energy $E_{\sigma_{120}} + E_{\sigma_m}$, is

$$d = \frac{4h^{3/2}}{b_{11} - b_{12}} \left[\frac{1}{2} \left(1 - \frac{\pi}{3\sqrt{3}} \right) (c_{11} - c_{12}) (A \cdot 2\pi M_0^2)^{3/2} \right]^{1/2},$$

which amounts to $\approx 16 \mu\text{m}$ at a plate thickness $h \approx 80 \mu\text{m}$ (the observed value is $\approx 20 \mu\text{m}$).

On certain sections of the plate there is observed a

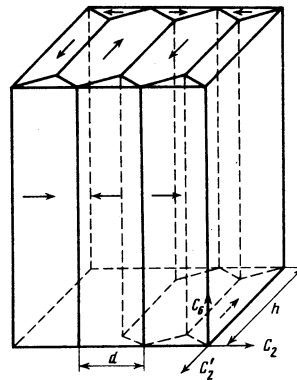


FIG. 6. Model of DS in nonaxial plate. EMA perpendicular to the plate surface.

strip DS that does not separate into layers parallel to the basal plane (see Figs. 1 and 2). We assume that in this region of the plate there exists one EMA perpendicular to the plane of the plate. In this case one can propose the DS model shown in Fig. 6. This structure is not separated into layers parallel to the basal plane, so that the latter do not have a combined magnetic moment. An estimate of the equilibrium domain size d yields

$$d = \frac{2\hbar^4}{b_{11}-b_{12}} [2(c_{11}-c_{12})(A \cdot 2\pi M_0^2)^{1/2}]^{1/4}.$$

Thus, the proposed models describe not only the main features of the DS in an RbNiF_3 plate, but also result in a domain-size estimate close to that observed in experiment, thus indicating that these features are realistic. In addition to the two cases considered, other variants of the EMA orientation relative to the plate surface are possible, and yield similar estimates of the domain sizes. A case when the EMA is parallel to the plane of the plate is not observed in experiment.

It should be noted that in exceptional cases an analysis of the domain structures observed on plates with different orientation can reveal the sign of the constant K_3 . As a rule, however, such an analysis is made very complicated by the influence of the residual stresses on the formation of the DS.

The authors thank B. A. Ivanov for a helpful discussion of the results.

¹Institute of Physics Problems, USSR Academy of Sciences.

¹G. S. Kandaurova and Y. V. Ivanov, *Zh. Eksp. Teor. Fiz.* **70**,

666 (1976) [*Sov. Phys. JETP* **43**, 343 (1976)].

²R. V. Pisarev, I. G. Siny, and G. A. Smolensky, *Solid State Commun.* **7**, 23 (1969).

³E. I. Golovenchits, A. G. Gurevich, and V. A. Sanina, *Pis'ma Zh. Eksp. Teor. Fiz.* **3**, 408 (1966) [*JETP Lett.* **3**, 266 (1966)].

⁴A. N. Grishmanovskii, *Fiz. Tverd. Tela (Leningrad)* **16**, 2716 (1974) [*Sov. Phys. Solid State* **16**, 1755 (1975)].

⁵W. Rüdorff, I. Kändler, and D. Babel, *Z. Anorg. Allgem. Chem.* **317**, 261 (1962).

⁶M. W. Shafer, T. R. McGuire, B. E. Argyle, and G. J. Fan, *Appl. Phys. Lett.* **10**, 202 (1967).

⁷E. I. Golovenchits, V. A. Sanina, and A. G. Gurevich, *Fiz. Tverd. Tela (Leningrad)* **10**, 2956 (1968) [*Sov. Phys. Solid State* **10**, 2334 (1979)].

⁸R. D. Burbank and H. T. Evans Jr., *Acta Cryst.* **1**, 330 (1948).

⁹A. I. Belyaeva, V. V. Eremenko, V. I. Silaev, R. A. Vaishnoras, and V. A. Potakova, *Fiz. Tverd. Tela (Leningrad)* **17**, 369 (1975) [*Sov. Phys. Solid State* **17**, 233 (1975)].

¹⁰V. I. Silaev, Yu. E. Stetsenko, A. I. Belyaeva, Yu. N. Stel'makhov, and G. S. Egizaryan, *Prib. Tekh. Éksp. No.* **5**, 228 (1979).

¹¹W. J. Tabor and F. S. Chen, *J. Appl. Phys.* **40**, 2760 (1969).

¹²S. V. Vonsovskii and Ya. S. Shur, *Ferromagnetizm (Ferromagnetism)*, Gostekhizdat, 1948, pp. 272 and 236.

¹³I. A. Privorotskii, *Usp. Fiz. Nauk* **108**, 34 (1972) [*Sov. Phys. Usp.* **15**, 555 (1973)].

¹⁴A. N. Grishmanovskii, V. V. Lemanov, G. A. Smolenskii, and P. P. Syrnikov, *Fiz. Tverd. Tela (Leningrad)* **14**, 2369 (1972) [*Sov. Phys. Solid State* **14**, 2050 (1973)].

¹⁵A. Hubert, *Theory of Domain Walls in Ordered Media* [Russ. transl.], Mir, 1977, pp. 47 and 74.

¹⁶J. Als-Nielsen, R. J. Birgenau, and H. I. Guggenheim, *Phys. Rev.* **B6**, 2030 (1972).

¹⁷E. M. Lifshitz, *Zh. Eksp. Teor. Fiz.* **15**, 97 (1945).

Translated by J. G. Adashko

Absorption of hypersound in stratifying solutions in the vicinity of the critical point

L. M. Sabirov, Ya. Turakulov, and T. M. Utarova

Samarkand State University

(Submitted 13 May 1980)

Zh. Eksp. Teor. Fiz. **79**, 2263–2269 (December 1980)

The scattered-light spectra were used to measure the temperature dependence of the amplitude coefficient α and the velocity v of hypersound near the critical temperature of critical-concentration solutions having an upper critical stratification point. The results of the measurement are compared with conclusions of the present-day theory. A mechanism due to the coupling between the fluctuations of the order parameter and the entropy fluctuations is considered in addition to the interaction of the acoustic mode with the diffusion mode.

PACS numbers: 43.20.Hq

1. INTRODUCTION

Second-order phase transitions near critical points are being investigated by various methods. The thermodynamic, optical, acoustic, and other properties of media in the vicinity of critical points have been the subject of many experimental and theoretical studies (see, e.g., the monographs and reviews¹⁻³). These investigations have shown that certain thermodynamic parameters and dynamic coefficients have singularities

near the critical point. In particular, the acoustic properties of a medium in the vicinity of a critical point undergoes substantial changes. A number of experimental studies^{4,5} have shown that as the critical temperature of a pure liquid and the critical stratification temperature T_c of solutions are approached, the ultrasound absorption coefficient increases noticeably. A theory of sound propagation in the critical region, with account taken of the coupling of the acoustic and diffusion modes of motion, was developed in Refs. 6